

Fermi Velocity Dependent Critical Current in Ballistic Bilayer Graphene Josephson Junctions

Amis Sharma¹, Chun-Chia Chen², Jordan McCourt²,
Kenji Watanabe³, Takashi Taniguchi³, François Amet⁴, Gleb Finkelstein²,
Ivan Borzenets^{1,*}

¹Department of Physics and Astronomy, Texas A&M University, College Station, 77843, TX, USA

²Department of Physics, Duke University, Durham, 27701, NC, USA

³Advanced Materials Laboratory, NIMS, Tsukuba, 305-0044, Japan

⁴Department of Physics and Astronomy, Appalachian State University, Boone, 28607, NC, USA

*Corresponding Author. E-mail: borzenets@tamu.edu

We perform transport measurements on proximitized, ballistic, bilayer graphene Josephson junctions (BGJJs) in the intermediate-to-long junction regime ($L > \xi$). We measure the device's differential resistance as a function of bias current and gate voltage for a range of different temperatures. The extracted critical current I_C follows an exponential trend with temperature: $\exp(-k_B T / \delta E)$. Here $\delta E = \hbar v_F / 2\pi L$: an expected trend for intermediate-to-long junctions. From δE , we determine the Fermi velocity of the bilayer graphene, which is found to increase with gate voltage. Simultaneously, we show the carrier density dependence of δE , which is attributed to the quadratic dispersion of bilayer graphene. This is in contrast to single layer graphene Josephson junctions, where δE and the Fermi velocity are independent of the carrier density. The carrier density dependence in BGJJs allows for additional tuning parameters in graphene-based Josephson Junction devices.

Ballistic graphene Josephson junctions (GJJs) have been widely utilized as a platform to study various interesting physics that arise at low temperatures from interactions between superconductors and normal metals [1–6]. The ballistic superconductor-normal metal-superconductor Josephson junction (SNSJJ) hosts Andreev bound states (ABS) which carry supercurrents across the normal region of the JJ; a disorder-free weak link and high transparency at the SN interface are necessary. Hexagonal Boron-Nitride (hBN) encapsulated graphene as the weak link enables highly transparent contacts at the interface whilst keeping graphene clean throughout the fabrication process [7]. Here, we study proximitized, ballistic, bilayer graphene Josephson junctions (BGJJs). Bilayer graphene devices (in contrast to monolayer) allow extra potential tunability via a non-linear dispersion relation, applied displacement field, or lattice rotation [6].

The critical current (I_C) of SNSJJ in the intermediate-to-long regime, where the junction length

(L) \geq superconducting coherence length (ξ_0), scales with temperature (T) as $I_C = \exp(-k_B T / \delta E)$. Here, $\delta E = \hbar \nu_F / 2\pi L$, an energy scale related to ABS level spacing [8–12]. Note that in the intermediate regime ($L \approx \xi_0$) δE is found to be suppressed [4]. A previous study of GJJs found that in this regime, the relation is held more precisely when ξ was taken into account along with L , that is: $\delta E = \hbar \nu_F / 2\pi(L + \xi)$ [8]. Monolayer graphene displays a linear dispersion relation, which results in a constant fermi velocity (ν_{F0}). Thus, in ballistic GJJs, δE remains independent of the carrier density. In comparison, bilayer graphene displays a quadratic dispersion relation at low energies. In BGJJs we studied, a back-gate voltage (V_G) controls the carrier density; and δE dependence on V_G is observed. Using δE , we extract Fermi velocity in bilayer graphene: it is seen that ν_F increases with V_G , and saturates to the constant value, ν_{F0} , of the monolayer graphene.

Our device consists of a series of four terminal Josephson junctions (on SiO_2/Si substrate) made with hBN encapsulated bilayer graphene contacted by Molybdenum-Rhenium (MoRe) electrodes. Bilayer graphene is obtained via the standard exfoliation method. It is then encapsulated in hexagonal Boron-Nitride using the dry transfer method [13]. MoRe of 80 nm thickness is deposited via DC magnetron sputtering. The resulting device has four junctions of lengths 400 nm, 500 nm, 600 nm, and 700 nm. The width of the junctions is 4 μm . The device is cooled in a Leiden cryogenics dilution refrigerator operated at temperatures above 1 K, and the measurements were performed using the standard four-probe lock-in method. A gate voltage V_G is applied to the Si substrate with the oxide layer acting as a dielectric, which allows modulation of the carrier density.[4, 8, 14–17]. Fig. 1(a) displays the differential resistance (dV/dI) map of the 400 nm junction at $T = 1.37$ K; we see zero resistance (black region) across all applied V_G indicating the presence of supercurrent. As the bias current I_{bias} is swept from negative to positive values, the junction first reaches its superconducting state at a value $|I_{bias}| = I_R$, known as re-trapping current. Then, as $|I_{bias}|$ is increased to higher positive values, the junction transitions to the normal state at $|I_{bias}| = I_S$, known as switching current. Fig. 1(a) shows that the junction can sustain larger region of critical current as we modulate the carrier density to higher values via V_G . Fig. 1(b) displays a line plot extracted from the dV/dI map which shows hysteresis in I_R and I_S . This is a commonly observed phenomenon in underdamped junctions [14, 18], or can also be attributed self-heating [15, 16, 19]. The critical current I_C of the junction is approximately I_S as found in switching statistics measurements, discussed in previous publications [8, 20–22].

Extracting the critical current I_C from the differential maps for different temperatures, we can see that I_C falls exponentially with inverse T (Fig. 2c) We also extract conductance of the junction in the normal regime ($I_{Bias} \gg I_C$). Fig. 2(b) shows this conductance (G) for 400 nm junction

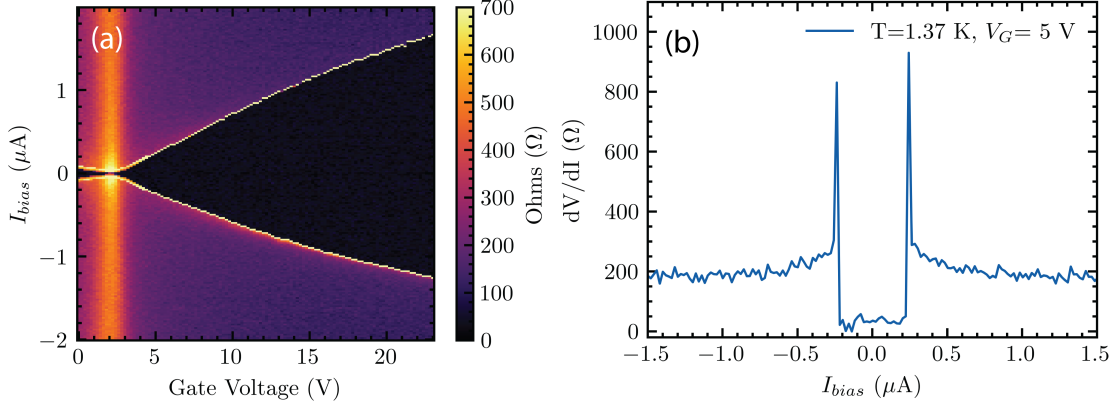


FIG. 1. (a) Differential resistance versus gate voltage (V_G) and bias current I_{Bias} taken at $T = 1.37$ K. The black region around zero bias corresponds to the superconducting state. I_{Bias} is swept from negative to positive. Thus, the transition at negative bias corresponds to the re-trapping current I_R , while the transition at positive bias is the switching current I_C . (b) Vertical line cut of the resistance map taken at $V_G = 5$ V, $T = 1.37$ K, showing device's differential resistance versus bias current.

device. We find that conductance G scales as the square-root of V_G as seen from the fit (blue curve). However, due to large contact resistance (R_C) of the device, the measured conductance G is suppressed compared to the ballistic limit expectation. Therefore, to demonstrate the ballistic nature of the device, we present normal resistances (R_N) of junctions of length 500 nm, 600 nm, and 700 nm (Fig. 2(c) inset). Taking into account R_C , we plot extracted values versus V_G from the Dirac point. The inset plot shows that the $R_N - R_C$ values are independent of junction length, which demonstrates the ballistic nature of the devices.

To extract δE of the junction, we go to the discussion of I_C vs temperature trends in Fig. 2(c). Here the y-axis is plotted in log scale. From the slope of curves $\text{Log}(I_C) = -(k_B/\delta E)T$ for each gate, one can extract δE versus V_G (plotted in Fig. 3a). Unlike for the case of monolayer graphene, a clear dependence on V_G is seen. The energy δE scales linearly with Fermi Velocity v_F (Fig. 3b). Note that calculating v_F from δE for junctions in the intermediate regime requires knowledge of the superconducting coherence length ξ . In our case ξ is obtained from the fit discussed below.

We now compare the experimentally obtained δE (and v_F) to the theoretical expectation. Assuming a quadratic dispersion relation $\mathcal{E}_F = \frac{\hbar^2 k_F^2}{2m^*}$, it follows that the expression for the Fermi velocity is: $v_F = \sqrt{\frac{2\mathcal{E}_F}{m^*}}$ [23–25]. The Fermi Energy \mathcal{E}_F for bilayer graphene scales as: $\mathcal{E}_F = \frac{\hbar^2 \pi |n|}{2m^*}$. With m^* being the effective mass of electrons in graphene. The carrier concentration n , controlled by the applied gate voltage V_G , is given by $n = \frac{V_G - V_d}{e} C_{Total}$ with V_d as the gate voltage at the Dirac point. The total capacitance C_{Total} is a combination of quantum capacitance C_q and gate oxide

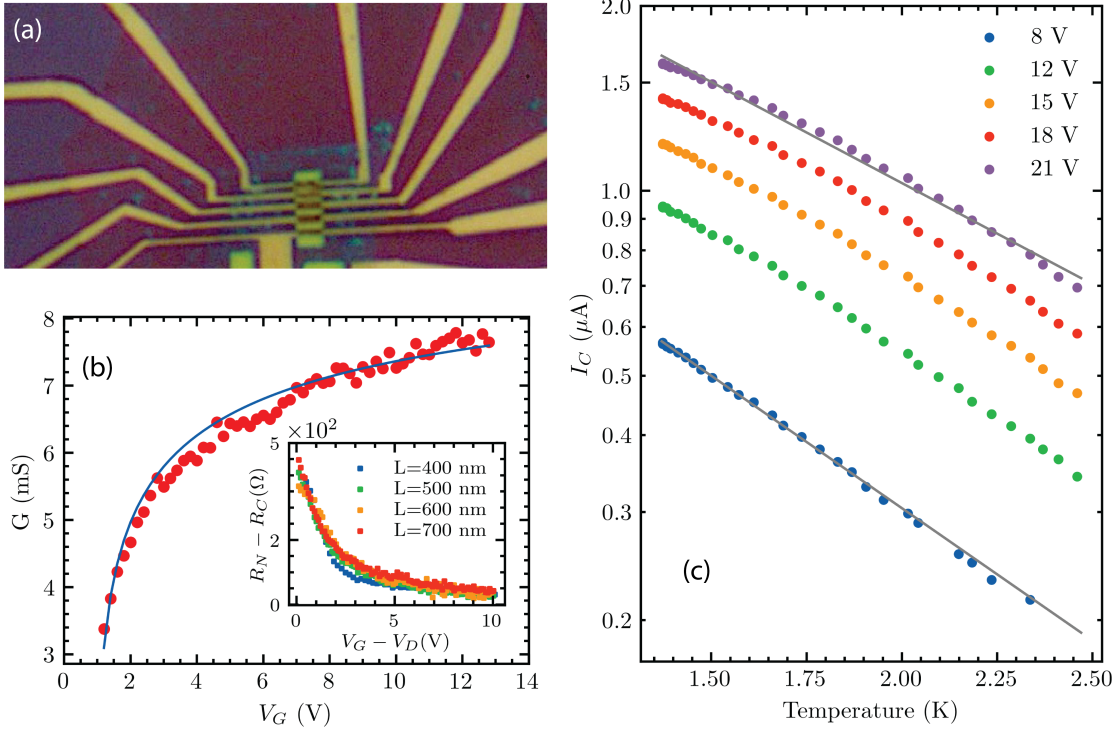


FIG. 2. (a) Device picture. Image shows series of junctions with different Lengths: 400 nm, 500 nm, 600 nm and 700 nm. (b) The ballistic conductance vs Gate voltage for $L = 400$ nm junction. The inset shows junction resistance minus the parasitic contact resistance plotted against gate voltage from the Dirac point for all our devices. (c) Critical currents I_C of $L = 400$ nm junction plotted against temperature T , for various gate voltages, on a semi-log scale. The plots show V_G dependence of I_C : the gray lines show that the slope of the curve for the lowest plotted gate $V_G = 8$ V, is smaller than the slope of the highest plotted gate $V_G = 21$ V.

capacitance C_{ox} : $C_{Total} = \left[\frac{1}{C_{ox}} + \frac{1}{C_q} \right]^{-1}$. The quantum capacitance C_q for bilayer graphene is determined by $C_q = \frac{2e^2 m^*}{\pi \hbar^2}$. The gate oxide capacitance per unit area is $C_{ox} = \frac{\epsilon_0 \epsilon_r}{d}$, where ϵ_0 is vacuum permittivity, ϵ_r is the relative permittivity of the oxide, and d is oxide layer thickness. For Silicon oxide gate with $d = 300$ nm we get $C_{ox} \approx 115 \mu F/m^2$. Thus, the full expression for the Fermi velocity v_F is:

$$v_F = \hbar \sqrt{\frac{2\pi\epsilon_0\epsilon_r e |V_G - V_d|}{m^*(2de^2m^* + \pi\epsilon_0\epsilon_r\hbar^2)}} \quad (1)$$

Note that the effective mass m^* typically ranges from $0.024 m_e$ to $0.058 m_e$ for $1 * 10^{12} \sim 4 * 10^{12}$ carriers/cm² [26], where m_e is the electron rest mass. Moreover, since m^* has a carrier concentration dependence, we assume a linear shift of m^* with the gate voltage as: $m^* = m_i + dm(V_G - V_d)$

[26].

Experimental data provides us with the following: $\delta E(V_G) = \frac{\hbar}{2\pi(L+\xi)}v_F$. To fit this data, the model is set as $\delta E(V_G) = \mathcal{F}(m_i, dm, \xi, V_d, d)$ where m_i, dm, ξ, V_d, d are the fitting parameters, and V_G is the independent variable. (We use the as-designed length of the device L , and take $\epsilon_r = 3.9$ for SiO_2 .)

The resulting fit of the data from the 400 nm junction for both δE and v_F is plotted as solid lines in Fig. 3(a) and Fig. 3(b) respectively. Moreover, taking the fitted ξ , we calculate the Fermi velocity v_F for all other junctions on the same substrate. As seen from Fig. 3(b), the calculated v_F of all devices is in good agreement with the fit obtained from the 400 nm junction. The fitted parameters are summarized in Table 1. All fall within the range of expected values, with ξ being consistent with previously measured values for graphene/MoRe junctions.

| Parameter | Fitted value | Expected Value |
|-----------|----------------|-------------------------|
| ξ | 460.34 nm | 300 ~ 500 nm |
| d | 317.71 nm | 300 ~ 330 nm |
| m_i | 0.020 m_e | 0.02 ~ 0.06 m_e |
| dm | 0.0003 m_e/V | 0.0002 ~ 0.0005 m_e/V |
| V_d | -1.99 V | $\approx \pm 2$ V |

TABLE I. The fitting parameters used to match the measured δE , and consequently the Fermi velocity v_F , versus gate to the theoretical expectation described in Equation 1. We see that resulting fitted values match closely to what is expected. The expected gate dielectric thickness d is estimated from the substrate specifications plus the bottom hBN thickness. The expected Dirac point voltage V_D is obtained from the resistance map. The expectations for the superconducting coherence length ξ and the effective mass m_i are obtained from previous works[4, 26].

In conclusion, we study the evolution of critical current with respect to gate in bilayer graphene Josephson Junctions (BGJJs). Using the critical current-temperature relation expected for intermediate-to-long junctions, we extract the relevant energy scale δE and find that it has a clear gate dependence. As δE is proportional to the Fermi velocity v_F in the bilayer graphene, we are able to match the observed gate dependence to the theoretical expectation. Our observation is contrasted with monolayer graphene JJs, that do not have a gate dependent δE . This result showcases the greater tunability of BGJJs, and offers additional avenues for device characterization.

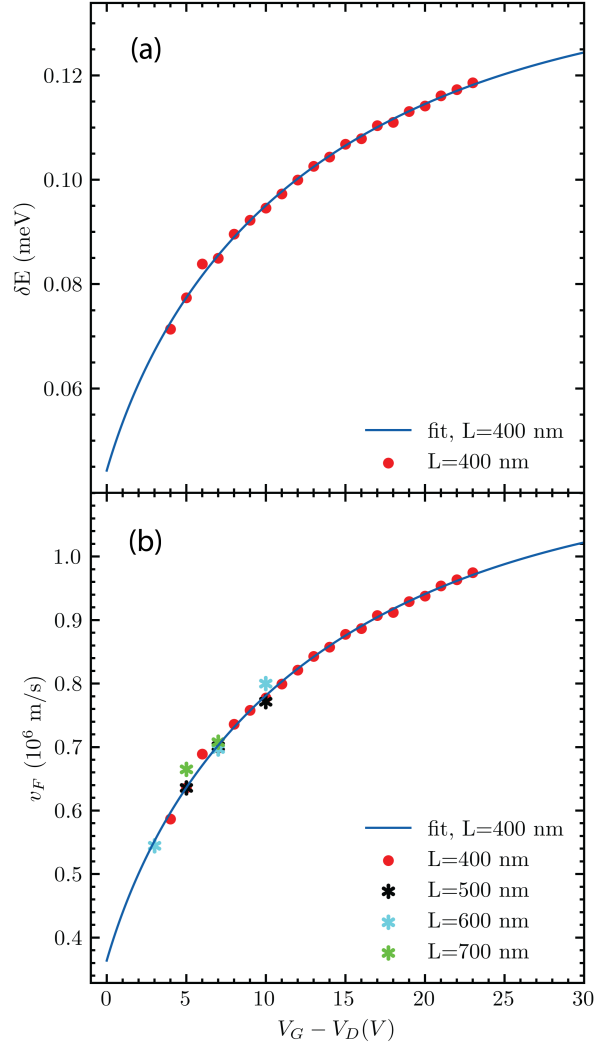


FIG. 3. (a) Energy δE extracted from the slope of $\log(I_C)$ vs T plotted against the gate voltage V_G from the Dirac point of the junction with $L = 400$ nm. We see δE dependence on the carrier density modulated via the gate voltage for the junction. (b) Fermi velocity (v_f) calculated from δE using the device dimensions, and the superconducting coherence length ξ obtained from the fit to theory. The solid line represents the theoretical trend as fitted to the data for the $L = 400$ nm junction. In addition, panel (b) shows calculated v_F for the other junctions using the ξ from the $L = 400$ nm fit.

-
- [1] W. Chen, D. N. Shi, and D. Y. Xing, Long-range cooper pair splitter with high entanglement production rate, *Scientific Reports* **5**, 10.1038/srep07607 (2015).
- [2] M. V. Feigel'man, M. A. Skvortsov, and K. S. Tikhonov, Proximity-induced superconductivity in graphene, *JETP Letters* **88**, 747 (2008).
- [3] Y. Shimazaki, M. Yamamoto, I. V. Borzenets, K. Watanabe, T. Taniguchi, and S. Tarucha, Generation and detection of pure valley current by electrically induced berry curvature in bilayer graphene, *Nature Physics* **11**, 1032–1036 (2015).
- [4] I. V. Borzenets, Y. Shimazaki, G. F. Jones, M. F. Craciun, S. Russo, M. Yamamoto, and S. Tarucha, High efficiency CVD graphene-lead (pb) cooper pair splitter, *Scientific Reports* **6**, 10.1038/srep23051 (2016).
- [5] J. G. Kroll, W. Uilhoorn, K. L. van der Eenden, D. de Jong, K. Watanabe, T. Taniguchi, S. Goswami, M. C. Cassidy, and L. P. Kouwenhoven, Magnetic field compatible circuit quantum electrodynamics with graphene josephson junctions, *Nature Communications* **9**, 10.1038/s41467-018-07124-x (2018).
- [6] G. H. Park, W. Lee, S. Park, K. Watanabe, T. Taniguchi, G. Y. Cho, and G. H. Lee, Controllable andreev bound states in bilayer graphene josephson junctions from short to long junction limits, *Physical Review Letters* **132**, 10.1103/physrevlett.132.226301 (2024).
- [7] C. R. Dean, A. F. Young, I. Meric, C. Lee, L. Wang, S. Sorgenfrei, K. Watanabe, T. Taniguchi, P. Kim, K. L. Shepard, and J. Hone, Boron nitride substrates for high-quality graphene electronics, *Nature Nanotechnology* **5**, 722 (2010).
- [8] I. V. Borzenets, F. Amet, C. T. Ke, A. W. Draelos, M. T. Wei, A. Seredinski, K. Watanabe, T. Taniguchi, Y. Bomze, M. Yamamoto, S. Tarucha, and G. Finkelstein, Ballistic graphene josephson junctions from the short to the long junction regimes, *Phys. Rev. Lett.* **117**, 237002 (2016).
- [9] I. O. Kulik, Macroscopic quantization and the proximity effect in s-n-s junctions, *Soviet Physics JETP* **30**, 944 (1970).
- [10] J. Bardeen and J. L. Johnson, Josephson current flow in pure superconducting-normal-superconducting junctions, *Physical Review B* **5**, 72–78 (1972).
- [11] A. V. Svidzinsky, T. N. Antsygina, and E. N. Bratus, *Soviet Physics JETP* **3**, 860 (1972).
- [12] A. V. Svidzinsky, T. N. Antsygina, and E. N. Bratus, *Journal of low Temperature Physics* **10**, 131 (1973).
- [13] L. Wang, I. Meric, P. Y. Huang, Q. Gao, Y. Gao, H. Tran, T. Taniguchi, K. Watanabe, L. M. Campos, D. A. Muller, J. Guo, P. Kim, J. Hone, K. L. Shepard, and C. R. Dean, One-dimensional electrical contact to a two-dimensional material, *Science* **342**, 614 (2013).
- [14] I. V. Borzenets, U. C. Coskun, S. J. Jones, and G. Finkelstein, Phase diffusion in graphene-based josephson junctions, *Physical Review Letters* **107**, 10.1103/physrevlett.107.137005 (2011).
- [15] I. V. Borzenets, U. C. Coskun, H. T. Mebrahtu, Y. V. Bomze, A. I. Smirnov, and G. Finkelstein,

- Phonon bottleneck in graphene-based josephson junctions at millikelvin temperatures, *Physical Review Letters* **111**, 10.1103/physrevlett.111.027001 (2013).
- [16] J. Tang, M. T. Wei, A. Sharma, E. G. Arnault, A. Seredinski, Y. Mehta, K. Watanabe, T. Taniguchi, F. Amet, and I. Borzenets, Overdamped phase diffusion in hbn encapsulated graphene josephson junctions, *Phys. Rev. Research* **4**, 023203 (2022).
- [17] F. Amet, C. T. Ke, I. V. Borzenets, J. Wang, K. Watanabe, T. Taniguchi, R. S. Deacon, M. Yamamoto, Y. Bomze, S. Tarucha, and G. Finkelstein, Supercurrent in the quantum hall regime, *Science* **352**, 966 (2016).
- [18] M. Tinkham, *Introduction to Superconductivity* (Dover Publications, 2004).
- [19] H. Courtois, M. Meschke, J. T. Peltonen, and J. P. Pekola, Origin of hysteresis in a proximity josephson junction, *Physical Review Letters* **101**, 10.1103/physrevlett.101.067002 (2008).
- [20] U. C. Coskun, M. Brenner, T. Hymel, V. Vakaryuk, A. Levchenko, and A. Bezryadin, Distribution of supercurrent switching in graphene under the proximity effect, *Physical Review Letters* **108**, 10.1103/physrevlett.108.097003 (2012).
- [21] G. H. Lee, D. Jeong, J. H. Choi, Y. J. Doh, and H. J. Lee, Electrically tunable macroscopic quantum tunneling in a graphene-based josephson junction, *Physical Review Letters* **107**, 10.1103/physrevlett.107.146605 (2011).
- [22] C. T. Ke, I. V. Borzenets, A. W. Draelos, F. Amet, Y. Bomze, G. Jones, M. Craciun, S. Russo, M. Yamamoto, S. Tarucha, and G. Finkelstein, Critical current scaling in long diffusive graphene-based josephson junctions, *Nano Letters* **16**, 4788–4791 (2016).
- [23] W. Zhu, V. Perebeinos, M. Freitag, and P. Avouris, Carrier scattering, mobilities, and electrostatic potential in monolayer, bilayer, and trilayer graphene, *Physical Review B* **80**, 10.1103/physrevb.80.235402 (2009).
- [24] T. Fang, A. Konar, H. Xing, and D. Jena, Carrier statistics and quantum capacitance of graphene sheets and ribbons, *Applied Physics Letters* **91**, 10.1063/1.2776887 (2007).
- [25] R. Fates, H. Bouridah, and J. P. Raskin, Probing carrier concentration in gated single, bi- and tri-layer cvd graphene using raman spectroscopy, *Carbon* **149**, 390–399 (2019).
- [26] K. Zou, X. Hong, and J. Zhu, Effective mass of electrons and holes in bilayer graphene: Electron-hole asymmetry and electron-electron interaction, *Physical Review B* **84**, 10.1103/physrevb.84.085408 (2011).